Control of Size and Composition of Colloidal Nanocrystals of Manganese Oxide

Gene M. Nolis, Jannie M. Bolotnikov and Jordi Cabana

Affiliation:

Department of Chemistry
University of Illinois at Chicago
Chicago, IL 60607, USA.
E-mail: jcabana@uic.edu

Abstract:

A comprehensive study on the effects of experimental parameters on the composition and size of manganese oxide nanocrystals was completed using colloidal chemistry. The reactions studied involved the thermolysis of Mn^{2+} acetate and Mn^{3+} acetylacetonate in oleylamine. Temperature was found to be the dominant factor affecting the composition and size of the products. Reactions completed below 200 ^{o}C favored the formation of nanocrystals smaller than 20 nm, with the presence of even impurity amounts of oxidizing agents leading to the formation of Mn_3O_4. Nanocrystals of MnO could only be synthesized below 200 ^{o}C if Mn^{2+} acetate was used, and the reaction was carefully controlled to have no O_2 and H_2O contamination. In turn, particle growth was rapid above this temperature. In this case, regardless of the oxidizing agents used or oxidation state of the Mn precursor, nanocrystals of MnO formed after annealing for at least one hour at temperatures higher than 200 ^{o}C. This finding suggests the role of oleylamine as solvent, surfactant and reducing agent at sufficiently high annealing temperatures. These results increase the understanding of redox stability of manganese during the colloidal synthesis of semiconductor metal oxide nanocrystals.

Introduction:

With the turn of the century, nanocrystals of manganese oxide have been touted for a variety of applications, such as wastewater treatment, magnetic imaging, catalysis, sensors, supercapacitors and rechargeable batteries, justified by the unique properties triggered at small sizes.[1–4] Specifically, in the case of batteries, the short lengths for diffusion of charge carriers enable faster kinetics of reactions in high capacity electrodes.[5,6] Such short lengths could be critical to enable battery concepts based on the intercalation of multivalent ions, such as Mg^{2+}, because of the high activation barriers and, thus, low coefficients for diffusion of these highly charged species. Batteries pairing an intercalation cathode and a Mg metal anode are predicted to surpass the density of energy of storage of commercial Li-ion technologies.[7] As a representative example, reversible, yet sluggish, intercalation of Mg^{2+} into spinel-type Mn_2O_4 was observed in micron-sized particles.[8] Motivated by computational studies suggesting that divalent cations could migrate sufficiently well in spinel lattices to sustain reversible electrochemical reactions at very small crystal sizes,[7] our group synthesized $Mg_{0.5}Mn_{2.5}O_4$ nanocrystals below 20 nm.[9] The materials were electrochemically active, but the existence of both Mg^{2+} and Mn^{2+} induced site exchange between both cations, resulting in the intercalation of both Mg^{2+} and Mn^{2+}. It was hypothesized that exclusive intercalation of Mg^{2+} could be achieved in stoichiometric, ordered $MgMn_2O_4$, where all of the Mn is in the +3 oxidation state.

Colloidal synthetic methods in the liquid phase provide a pathway to consistently control the particle size, shape and size distribution of nanocrystals.[1,10] In a typical colloidal synthesis, salts of metals are decomposed in high-boiling point surfactant/solvent to yield crystalline dispersions of nanoparticles. However, Mn_3O_4 is the oxide with the highest average oxidation state of Mn (+2.66) reportedly made under colloidal conditions, even in the presence of soft oxidizing agents, such as trimethylamine N-oxide dihydrate.[11–15] Given that targeting compounds such as ordered nanoscale $MgMn_2O_4$ clearly challenges current synthetic capabilities, a comprehensive understanding is required of the effect and limits of chemical parameters on the specific Mn-O phase forming in a colloidal environment.

Several reports exist where carboxylate salts (e.g. formate, acetate, acetylacetonate) of Mn^{2+} were thermally decomposed in oleylamine or oleylamine-based solvents to obtain nanocrystals of MnO or Mn_3O_4.[12–16] Jiao *et al.* observed that thermolytic decomposition of Mn^{2+} acetylacetonate [$Mn(acac)_2$] in oleylamine at 210 ^{o}C, while exposed to normal atmosphere, resulted in nanocrystals of Mn_3O_4 capped with an Mn^{4+} shell.[12] The shell of Mn^{4+} was ascribed by the authors to the presence of O_2 in the atmosphere. In contrast, other groups conducted reactions

protected from unwanted O_2 and H_2O by flowing a blanket of inert gas (N_2 or Ar) over the ongoing reaction, enhanced by evacuating the reaction vessel. Nanocrystals of pure Mn_3O_4 are reportedly favored when annealing carboxylate precursors of Mn^{2+} under O_2- and H_2O-free conditions at temperatures from 100 to 250 ^oC, for up to 10 hours.[13–15] It has been hypothesized that MnO forms initially but is later oxidized by CO_2 to form Mn_3O_4. As a contrast, Seo *et al.* described the formation of nanocrystals of pure MnO at annealing temperatures of 220 – 250 ^oC. In this case, the reactions were conducted with the controlled addition of H_2O within the same general conditions.[13] The authors argued that the presence of H_2O prohibits oxidation of MnO to Mn_3O_4. In yet a separate study, Zhang *et al.* reported that annealing Mn^{2+} acetate [$Mn(ac)_2$] at 250 ^oC, without H_2O, could result in the formation of nanocrystals of either mixed phase Mn_3O_4/MnO or pure MnO, depending on the specific heating protocol.[14] In contrast, during the thermolytic decomposition of Mn^{2+} formate at 340 ^oC, Ould-Ely *et al.* determined that nanocrystals of pure MnO formed with and without H_2O, generating a seeming contradiction in the literature.[16] This observation is consistent with other studies where formation of crystalline nanocrystals of MnO was found following the thermal decomposition of $Mn(ac)_2$ in the presence of oleic acid, rather than oleylamine, at 320 ^oC.[11,17] Most importantly, despite the expected generation of CO_2 upon thermolysis of the carboxylate precursor, these nanocrystals of MnO could only be oxidized to Mn_3O_4 by adding a mild oxidizer, trimethylamine-N-oxide (TMNO).[11] This oxidative method was adapted from the seminal work by Hyeon *et al.* where colloidally prepared nanoparticles of Fe were uniformly transformed to monodisperse Fe_2O_3 by controlled oxidation using the same reagent.[18] Despite this broad synthetic effort, to date, there has been no systematic study of the decomposition of Mn^{3+} precursors in oleylamine, so the possibility of synthesizing Mn_2O_3 instead of Mn_3O_4 has not be fully probed. Lastly, no report exists of a surfactant-assisted colloidal reaction that produces nanoscale MnO_2 (Mn^{4+}).

With the dual goal of providing a resolution to the conflicting results in the literature desibed above, and, broadly, evaluate the level of control over Mn oxidation state in colloidal conditions, this report evaluates effects of temperature and oxidizing conditions on products following the thermal decomposition of $Mn(ac)_2$ and $Mn(acac)_3$ in oleylamine during a one-step heat-up colloidal method. Powder X-ray diffraction and transition electron microscopy techniques were used to characterize the composition and morphology of all nanocrystalline products. By carefully controlling experimental conditions, an enhanced understanding of what factors (*i.e.* temperature, oxidizing agent, H_2O, etc.) are critical in governing the oxidation state of Mn and nanocrystal size of the product is provided. These results provide important insights into the redox activity of transition metals in colloidal synthesis of crystalline metal oxide nanoparticles.

Experimental Methods:

All experiments were carried out using standard Schlenk techniques under nitrogen atmosphere. $Mn(ac)_2$ (98 %), $Mn(acac)_3$ (technical grade), and trimethylamine N-oxide dihydrate (TMNO, 98 %) were purchased from Sigma-Aldrich and used without further purification. Oleylamine (Sigma-Aldrich, 70 % pure) was also used without additional purification.

In a typical heat-up synthesis, a mixture of either $Mn(ac)_2$ or $Mn(acac)_3$ and oleylamine in a molar ratio of 1:12 Mn to oleylamine was prepared in a three-neck round bottom flask. For each Mn salt, reactions were completed either under inert atmosphere or in air. In the former case, reactions were conducted with and without a mild oxidizer, TMNO. To ensure inert conditions, the reaction flask was capped in the Schlenk line, and evacuated under constant stirring at room temperature until bumping ceased. The reaction slurry was then heated to 100 ^oC; whereupon the flask was degassed at least twice until bubbling ceased. Longer times were needed to degas the reaction with TMNO because the salt contained crystalline H_2O. To carry out the synthesis in air, the reaction mixture was left under constant magnetic stirring and exposed to laboratory

atmosphere. Following the proper pre-reaction setup for each type of reaction, the flask was rapidly heated to 150, 200, 250 or 300 °C, and held at that temperature, followed by cooling to room temperature. After the addition of 30 mL of a polar organic solvent, the product was centrifuged and the supernatant was separated off. The process was repeated twice with 10 mL of hexane and 20 mL of non-polar solvent to remove the remaining unreacted surfactant. The resulting powder was dried overnight at 60 °C.

Thermogravimetric analysis (TGA) and differential scanning calorimetry (DSC) experiments were completed using a TA Instruments SDT Q600. Powder precursors were heated to 320 °C at a heating rate of 5 °C per minute, following a 30-minute isotherm at 50 °C. A 30-minute isothermal step at 50 °C was added to promote complete saturation of the reaction chamber with the gas used. Separate experiments were completed using either synthetic air or N_2 (Praxair). Upon reaching 320 °C, the temperature was maintained for two hours before cooling.

In-house powder X-ray diffraction (PXRD) was performed on a Bruker D8 Advance using Cu Kα (λavg = 1.5418 Å) radiation. Scan rates were 0.04° s−1 from 10° to 80° (2θ). The XRD patterns of harvested electrodes were aligned by linearly shifting them based on the position of the (220) peak of stainless steel (JCPDS card number: 33–397, austenitic $Fe_{0.70}Cr_{0.19}Ni_{0.11}$), which was used as an internal standard.

Transmission electron microscopy (TEM) was completed using a JEM 3010 (JEOL) operated at 300 kV. The samples were prepared by taking a small aliquot of powder sample and sonicating in chloroform for at least 30 minutes. Then, using a pipette, the sample was drop-casted onto a 200 x 200 mesh copper TEM grid with an amorphous carbon layer. At least three drops were casted.

Results:

Thermal decomposition of Mn^{2+} acetate

Dry powder of $Mn(ac)_2$ showed prominent decomposition events at 250 and 280 °C when heated in a TGA/DSC apparatus under synthetic air (exothermic, -55.5 J) or N_2 (endothermic, 11.0 J) atmosphere, respectively (Figure 1a,c). PXRD was used to determine the crystal structure and quality of the decomposition products. Pawley fits were used to correlate experimental PXRD data to standard crystal structures and determine unit cell parameters. The product of decomposition in synthetic air was pure Mn_3O_4 (space group *I41/amd*, a = 5.75 Å and c = 9.42 Å) and showed a 56 % reduction in mass (theoretical loss, 56 %). On the other hand, pure MnO (space group *Fm-3m*, a = 4.43 Å) was produced in N_2 (Figure 1b,d) and was accompanied by an mass reduction of 60 % (theoretical loss, 60 %). Since MnO formed under inert conditions, CO_2 formed from decomposition of the ligand does not oxidize Mn^{2+}, as previously claimed.[15] On the other hand, in the presence of O_2 in air, decomposition of $Mn(ac)_2$ will occur through partial oxidation of Mn^{2+} to Mn^{3+} to form Mn_3O_4.

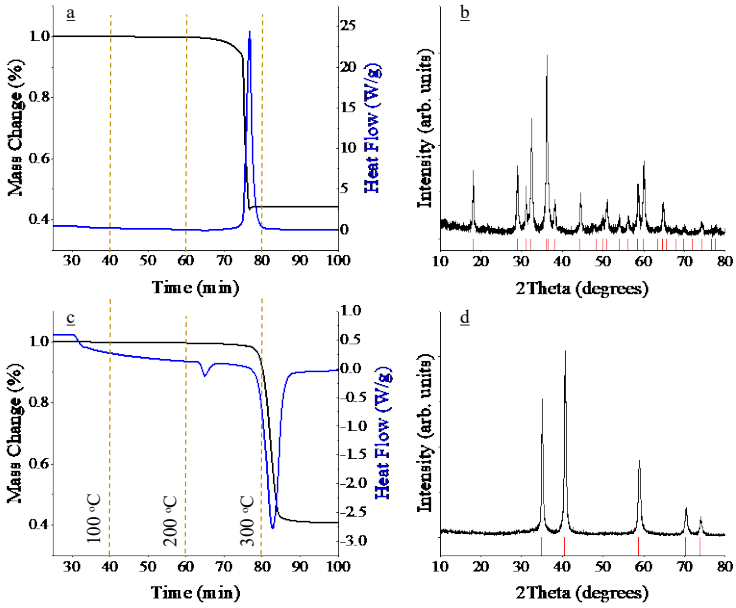

Figure 1. Thermal gravimetric analysis (black line) and differential scanning calorimetry (blue line, exo up) plots following heating of $Mn(ac)_2$ powder in synthetic air (a) or N_2 (c) atmospheres. Powder X-ray diffraction patterns of the corresponding products of decomposition in synthetic air (b) and N_2 (d) atmospheres are also shown, respectively. Red tick marks correspond to reflections of spinel Mn_3O_4 (b) and cubic MnO (d). Orange dashed lines correspond time of experiment to temperature, where 40, 60, 80 and 84 min are equivalent to 100, 200, 300 and 320 °C.

Manganese oxide nanocrystals were prepared by thermally decomposing $Mn(ac)_2$ in oleylamine, as described in the experimental section. During a series of "control" thermolysis reactions, the round-bottom flasks (reaction vessels) were purged with N_2 gas and kept air-tight, completely free of O_2 and H_2O, in a Schlenk line. Usually, the reaction solution was transparent with a slight yellow color after a successful degas regimen, which later turned green (sometimes grey). PXRD patterns of the products of the thermal decomposition of $Mn(ac)_2$ in oleylamine from 200 – 300 °C (Figure 2a) revealed the formation of crystalline MnO, consistent with color changes. MnO is commonly found in nature as the green mineral manganosite. The large peak widths are indicative of the production of nanocrystals. These results indicate that the $Mn(ac)_2$ preferentially decomposes to form MnO in the absence of O_2 and H_2O, supporting TGA results. No product formed after 1 h of decomposition at 150 °C under inert conditions. Longer reaction times, 6-12 h, were needed to produce crystalline MnO (Figures 2a and S1). The reaction time to form MnO nanocrystals could be reduced to 3 h if the temperature of decomposition was raised by 25 °C to 175 °C (Figure S2a). Zhang *et al.* reported need to decompose $Mn(ac)_2$ for 10 hours at 100 °C to form highly crystalline nanoparticles of Mn_3O_4.[14] These annealing temperatures are much lower than 280 °C (endothermic event associated with MnO formation in Figure 1c) inferring that colloidal reaction thermodynamics were different than in solvent-free environments, possibly due to the formation of different Mn^{2+} complexes involving oleylamine prior to thermolysis. In turn, long reaction times (slow rates) are likely the result of slow kinetics of decomposition of the precursor, $Mn(ac)_2$, at temperatures close to the thermodynamic value in these conditions. The results were unexpected since other reports indicate when decomposing Mn^{2+} precursor salts under O_2- and H_2O-free conditions in oleylamine at temperatures of 100 - 250 °C nanocrystals of Mn_3O_4 are produced.[13–15] These reports claim that CO_2, a byproduct of ligand decomposition, acts as the main oxidizing source. The results presented here suggest that

CO_2 is insufficiently oxidizing and that inert conditions successfully preserve Mn^{2+} during thermolysis. More than likely, O_2 contaminated these reactions in the literature, favoring the formation of Mn_3O_4.

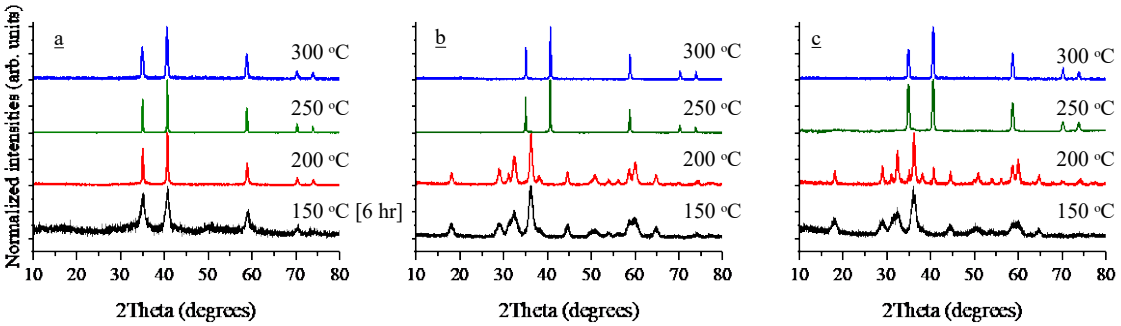

Figure 2. Powder X-ray diffraction of as-prepared nanocrystals following thermal decomposition of $Mn(ac)_2$ in oleylamine as a function of temperature in, (a) N_2, (b) air or (c) N_2 with TMNO. Diffraction peak intensities were normalized. All reactions were carried out for 1 hour, unless otherwise noted.

The decomposition of $Mn(ac)_2$ for 3 h at 175 °C under inert conditions was exemplary of the need to carefully control synthetic conditions to produce the desired compound. It was found to be extremely sensitive to the order in which the reaction mixture was prepared in the round bottom flask. Mn_3O_4 formed when $Mn(ac)_2$ was first added to the reaction vessel followed by oleylamine and a series of generic thirty-minute degas steps (Figure S2a); the solution turned brown instead of green. Even if a protective N_2 blanket was employed, the solution always turned brown by the time $Mn(ac)_2$, a pink powder, had dissolved into oleylamine (Figure S2b). The dramatic change of the color of the solution from transparent to an opaque brown at room temperature suggests that the Mn-O-oleylamine complex is sensitive to oxidizing impurities in the vessel, and likely reacted prior to degassing and heating. Zhang *et al.* also observed this phenomenon when they dissolved $Mn(ac)_2$ into oleylamine.[14] More than likely, O_2 trapped in the salt and under the oleylamine contaminates the reaction and oxidizes the Mn^{2+}-oleylamine complex. Throughout our experiments, we found that adding the precursor salt to the reaction vessel already filled with oleylamine, and under a nitrogen blanket, reduced the presence of Mn_3O_4 in the end-product. Still, the solution would turn brown in some cases, compromising control of the reaction. Therefore, a single degas step at room temperature was added to the synthetic procedure in order to quantitatively remove O_2 and H_2O prior to heating. The degas was considered complete after bumping of the volatile impurities from the reaction mixture stopped; whereupon the solution would turn transparent with a slight yellow color by the time the system reached 100 °C (Figure S2c). Then, crystalline MnO nanoparticles were reproducibly obtained when all these steps were implemented, which were adapted for all other reactions under inert N_2 and N_2 with TMNO (Figures 1a,c and S2d).

A dramatic change in the decomposition of $Mn(ac)_2$ was observed when the reaction was conducted in air, in the laboratory atmosphere, Mn_3O_4 readily and consistently formed after one hour of decomposition at 150 and 200 °C (Figure 2b). During these experiments, as the precursor salts dissolved into the surfactant, the solution turned brown, as expected from Mn_3O_4. Mn_3O_4 is commonly found in nature as a brown mineral hausmannite. Jiao *et al.* also found that decomposing $Mn(acac)_2$ in oleylamine at 210 °C in air yielded nanocrystals of Mn_3O_4.[12] Oxidation of Mn^{2+} to Mn^{3+}, and subsequent formation of Mn_3O_4, is expected since this product formed after heating $Mn(ac)_2$ in air in the TGA apparatus (Figure 1b). However, referring back to Figure 2b, MnO was formed when the colloidal reaction was performed in air at 250 and 300 °C.

These results indicate Mn^{3+} is only stable at annealing temperatures lower than 250 °C, probably because it oxidizes oleylamine at higher temperature. The critical role of oxidizing agents in the formation of Mn_3O_4 over MnO was further confirmed by decomposing $Mn(ac)_2$ in oleylamine under N_2 in the presence of TMNO, a mild oxidizing agent. In accordance to the diffraction patterns in Figure 2c, pure Mn_3O_4 formed after annealing for 1 h at 150 °C. A product with mixed MnO/Mn_3O_4 phases formed after the reaction completed at 200 °C. Finally, pure MnO resulted from the decomposition at 250 and 300 °C. Exposure to TMNO (Figure 2c) and atmospheric sources of O_2 (Figure 2b) favor the formation of pure Mn_3O_4 nanocrystals during pyrolysis of $Mn(ac)_2$ in oleylamine at 150 °C. These results support the notion that Mn^{3+} is stable in the presence of an oxidizer only at reaction temperatures of 200 °C or less. Oleylamine is known to act as an electron donor at elevated temperatures.[19] This surfactant contains a C=C bond that is liable to break given enough force. Oxidation of the C=C bond is likely accelerated by thermal energy and the presence of Mn^{3+}. The presence of both phases of MnO and Mn_3O_4 at 200 °C suggests it is the temperature where a transition to reducing conditions occurs.

The large peak widths observed in the PXRD patterns (Figure 2) allude to the nanocrystalline nature of the samples, which was confirmed by transition electron microscopy (TEM, Figure 3). At least 300 particles from each colloidal synthesis reaction were measured from the TEM images (Figure S3) to build histograms (Figure S4) of particle size distributions. From the histograms, average particle sizes and error (taken as one standard deviation) were calculated, listed in Table 1, and plotted in Figure 3a. TEM images in Figure 3b-e correspond to nanocrystalline products formed after annealing $Mn(ac)_2$ in oleylamine in air (see Figure 2b for PXRD). They are representative of all the materials made in the study (Figure S3).

During the colloidal reactions, temperature had a measurable impact on particle size. While no particles could be collected annealing at 150 °C for 1 h under simply N_2, quasi-cubes of 8 ± 1 and rice-shaped 10 ± 2 nm nanocrystals of Mn_3O_4 were produced in the presence of TMNO and air, respectively (Figure 3a and Table 1). Decomposition of $Mn(ac)_2$ in oleylamine at 150 °C for 6 h (Figure 4a,c) and 175 °C for 3 h (Figure 4b,d) resulted in 7 ± 2 and 8 ± 3 nm MnO particles, respectively. Increasing the reaction temperature generally resulted in larger nanocrystals for each heat-up synthesis. Rice-shaped nanocrystals of Mn_3O_4 of 20 ± 6 and 10 ± 5 nm were produced after annealing $Mn(ac)_2$ at 200 °C in N_2 with TMNO and air, respectively. During the control experiments, 40 ± 8 nm truncated cubes of MnO were formed after one hour of thermolysis of $Mn(ac)_2$ at 200 °C. Annealing for one hour at 250 °C under inert, TMNO or air-oxidizing conditions resulted in 100 ± 30, 100 ± 100, and 70 ± 60 nm truncated cubes of MnO, respectively. Furthermore, annealing $Mn(ac)_2$ for one hour at 300 °C under inert, TMNO or air-oxidizing conditions resulted in 70 ± 20, 300 ± 80, and 100 ± 20 nm truncated cubes of MnO, respectively. Large standard deviations from the mean particle size at reactions completed at 250 °C, with TMNO or air, are associated with bimodal size distributions (Figure S4). These bimodal distributions in particle size growth are due to coarsening and/or Otswald ripening where larger nanoparticles grow at the expense of smaller ones. The particle size distributions in this report are all larger than ±5 % of the mean size, which does not satisfy the condition to claim monodispersity.[20] To improve monodispersity during heat-up syntheses, researchers report having to work in highly dilute conditions, add additional solvents/surfactants, or use different annealing/aging treatments.[11,13–15,17,18] These strategies would constitute a worthwhile endeavor for follow-up studies, but were considered beyond the scope of this work, which is to evaluate the level of control over Mn oxidation state in colloidal conditions, and its relationship with crystal size.

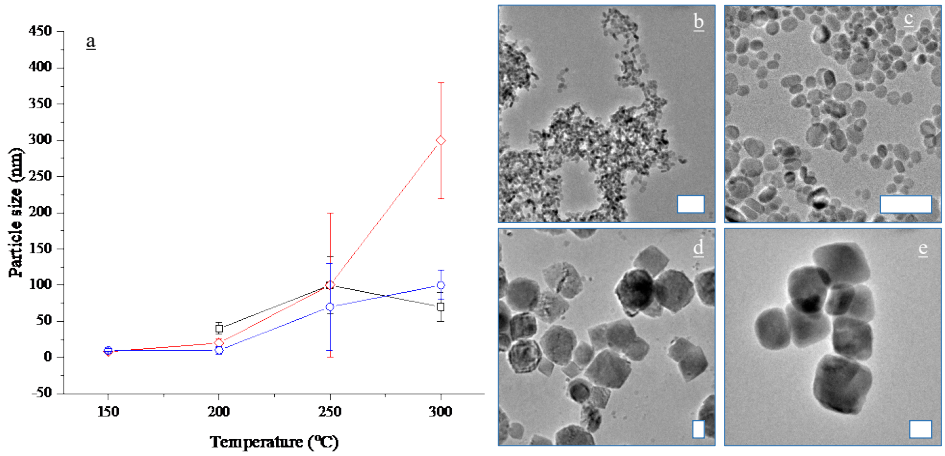

Figure 3. (a) Size distribution of nanoparticles produced after thermally decomposing $Mn(ac)_2$ in oleylamine. Squares, diamonds and circles correspond to reactions in N_2, N_2 with TMNO and air. Representative transmission electron microscopy images of products of the reactions under air, at (b) 150, (c) 200, (d 250, and (e) 300 °C. White scale bars correspond to 50 nm.

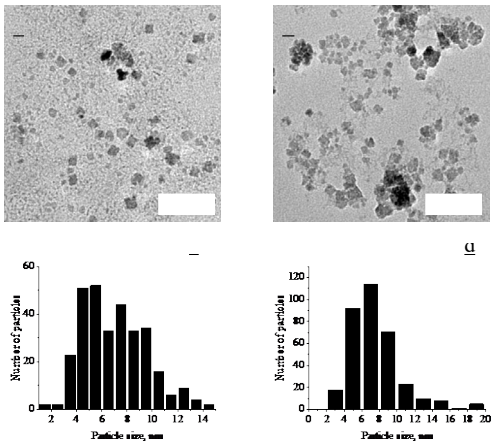

Figure 4. Transmission electron microscopy images and histograms of particle size distributions following thermolysis of $Mn(ac)_2$ in oleylamine for (a,c) six hours at 150 °C and (b,d) three hours at 175 °C under N_2.

Table 1. Summary of particle size and structure of as-prepared nanocrystals.

Precursor	Temperature	Oxidizing agent	Product	Particle size	Standard deviation
$Mn(ac)_2$	150	None	None	-	-
$Mn(ac)_2$	200	None	MnO	40	8
$Mn(ac)_2$	250	None	MnO	100	30

$Mn(ac)_2$	300	None	MnO	70	20
$Mn(ac)_2$	150	TMNO	Mn_3O_4	8	1
$Mn(ac)_2$	200	TMNO	MnO/Mn_3O_4	20	6
$Mn(ac)_2$	250	TMNO	MnO	100	100
$Mn(ac)_2$	300	TMNO	MnO	300	80
$Mn(ac)_2$	150	Air	Mn_3O_4	10	2
$Mn(ac)_2$	200	Air	Mn_3O_4	10	5
$Mn(ac)_2$	250	Air	MnO	70	60
$Mn(ac)_2$	300	Air	MnO	100	20
$Mn(acac)_3$	150	None	Mn_3O_4	8	2
$Mn(acac)_3$	200	None	Mn_3O_4	8	2
$Mn(acac)_3$	250	None	MnO	20	6
$Mn(acac)_3$	300	None	MnO	30	9
$Mn(acac)_3$	150	TMNO	Mn_3O_4	9	3
$Mn(acac)_3$	200	TMNO	MnO/Mn_3O_4	20	10
$Mn(acac)_3$	250	TMNO	MnO	60	30
$Mn(acac)_3$	300	TMNO	MnO	70	30
$Mn(acac)_3$	150	Air	Mn_3O_4	10	3
$Mn(acac)_3$	200	Air	Mn_3O_4	10	4
$Mn(acac)_3$	250	Air	MnO	20	10
$Mn(acac)_3$	300	Air	MnO	50	20

Thermal Decomposition of Mn^{3+} acetylacetonate

After the conditions for control of chemistry and nanocrystal size of manganese oxides made by thermolysis of $Mn(ac)_2$ were explored, it was determined that it is impossible to synthesize nanocrystals of pure Mn_2O_3. To try and prepare this product, a precursor with Mn in the 3+ oxidation state was chosen, namely Mn^{3+} acetylacetonate [$Mn(acac)_3$]. Also, to prevent any contamination by H_2O, an anhydrous salt of $Mn(acac)_3$ was used for this study. $Mn(acac)_3$ was heated in a TGA apparatus to 320 ^oC under synthetic air or N_2 atmosphere. The procedures resulted in exothermic (-61.4 J) and endothermic (0.6 J) decomposition events at temperatures between 170 and 250 ^oC (Figure 5a,c), respectively. PXRD patterns of the decomposition products in air consisted of pure Mn_3O_4 (Figure 5b,d), accompanied by an reduction in mass of 77 % (theoretical loss, 78 %). Bragg reflections associated with crystalline MnO were detected after decomposition in N_2 atmosphere. After thermal decomposition in N_2 atmosphere there was a 56 % loss in mass, which was much less than the expected loss of 80 %. $Mn(acac)_3$ is incredibly

stable and temperatures greater than 500 °C are needed to fully decompose it under inert atmosphere.[21] When thermolysis of $Mn(acac)_3$ was carried out in oleylamine, Mn_3O_4 was produced after one hour of annealing at 150 and 200 °C, regardless of conditions (Figure 6). Following decomposition under N_2 with TMNO at 200 °C, Mn_3O_4 was mixed with MnO (Figure 6c). Compared to similar heat-up synthesis with $Mn(ac)_2$, the only differences were observed at under rigorously inert conditions, where the use of a Mn^{3+} precursor led to Mn_3O_4 instead of MnO. In the case of 150 °C, the change in precursor also induced a reaction with accelerated the kinetics, as oxide nanoparticles could be collected after just one hour of annealing under inert conditions.

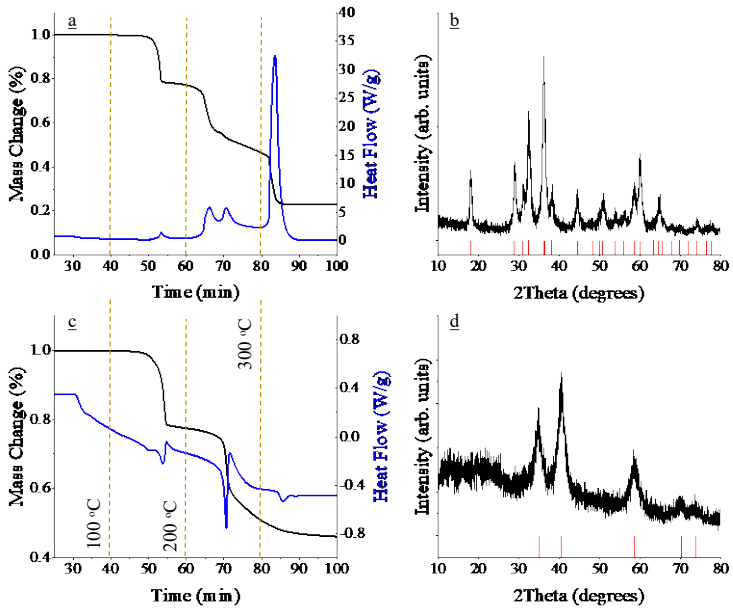

Figure 5. Thermal gravimetric analysis (black line) and differential scanning calorimetry (blue line, exo up) plots following heating of $Mn(acac)_3$ powder in synthetic air (a) or N_2 (c) atmospheres. Powder X-ray diffraction patterns of the corresponding products of decomposition in synthetic air (b) and N_2 (d) atmospheres are also shown, respectively. Red tick marks correspond to standard reflections of the crystallographic planes of spinel Mn_3O_4 (b) and cubic MnO (d). Orange dashed lines correspond time of experiment to temperature, where 40, 60, 80 and 84 min are equivalent to 100, 200, 300 and 320 °C.

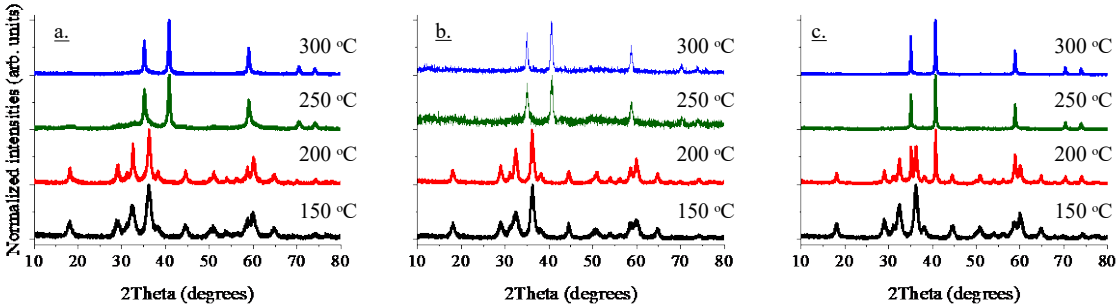

Figure 6. Powder X-ray diffraction of as-prepared nanocrystals following thermal decomposition of $Mn(acac)_3$ in oleylamine as a function of temperature in, (a) N_2, (b) air or (c) N_2 with TMNO. Diffraction peak intensities were normalized.

Figure 6 also shows that the products of thermolyzing $Mn(acac)_3$ at either 250 or 300 ^oC for one hour, regardless if the reaction was assisted by oxidizing agents or inert, always resulted in the formation of MnO nanocrystals. These results allude to the tripe role of oleylamine as solvent, surfactant and reducing agent since all Mn^{3+} in the precursor $Mn(acac)_3$ reduced to MnO (Mn^{2+}). They build upon a body of work in the literature, where oleylamine has been shown to reduce other trivalent transition metal acetylacetonate precursors ($Co(acac)_3$ and $Fe(acac)_3$) to their pure monoxide phases (CoO and FeO) during colloidal syntheses at annealing temperatures of 200 ^oC or greater.[22,23] During the decomposition of $Mn(acac)_3$, reactions were consistently brown upon heating, suggesting that the discrepancy between dry heating and thermolysis in oleylamine is not due to a complete reduction of Mn^{3+} to Mn^{2+} during the early stage of Mn-O-oleylamine complex formation. To understand this process better, an aliquot of the reaction solution was taken during the thermolysis of $Mn(acac)_3$ at 250 ^oC in air after 30 min. PXRD revealed that the washed product was composed purely of Mn_3O_4 (Figure S5). Further annealing, for a total of one hour, resulted in pure MnO (Figure 6b and Figure S5). From these results it is logical that upon heating, the Mn-O-oleylamine complex decomposed to favorably form Mn_3O_4 nanocrystals at low temperature in air. Then, after maintaining a reaction temperature of at least 250 ^oC for one hour, Mn_3O_4 reduces totally to MnO nanocrystals. These results indicate that oleylamine acts with a triple role, solvent, surfactant, and reducing agent; likely due to the existence of a C=C bond that is liable to donate electrons upon heating.[19] It is possible that the reducing character of oleylamine assists in the reduction of Mn^{3+} to form Mn_3O_4 even at temperatures as 150^oC, leading to a reaction that involves fast kinetics of product formation.

A global overview of particle sizes and size distributions of the decomposition products of $Mn(acac)_3$ in oleylamine is shown in Figure 7a and recorded directly in Table 1. Figure 7a reflects histograms (Figure S6) determined by counting at least 300 particles in TEM images (Figure S7). Figures 7b-e correspond to TEM images of the nanocrystalline products formed after annealing $Mn(acac)_3$ in oleylamine for one hour from 150 – 300 ^oC, which are representative of other samples at similar temperatures. Pure Mn_3O_4 nanocrystals produced in these reactions were more or less similar in size. After one hour of decomposition at 150 ^oC in N_2, N_2 with TMNO, and in air, the diameters of the Mn_3O_4 particles were 8 ± 2, 9 ± 3, and 10 ± 3 nm, respectively, and spherical in shape. The most significant crystal growth occurred above 200 ^oC, followed by a simultaneous transformation of the rice-shaped Mn_3O_4 to quasi-cubes of MnO. At 250 and 300 ^oC in N_2, particles had measured diameters of 20 ± 6 and 30 ± 9 nm, respectively. By allowing air to enter the reaction environment, nanocrystals of MnO of 20 ± 10 and 50 ± 20 nm were produced, respectively. The use of air did not significantly change the size of the nanocrystals of MnO. However, the diameters of nanocrystals of MnO were measured to be 60 ± 30 and 70 ± 30 nm following thermal decomposition of $Mn(acac)_3$ in the presence of TMNO at 250 and 300 ^oC. This increase in nanoparticle diameter is consistent with TEM analysis of $Mn(ac)_2$ decomposed in the presence of TMNO. Also, the diameter of the MnO nanocrystals at higher decomposition temperatures were found to be smaller than those formed using the precursor of $Mn(ac)_2$.

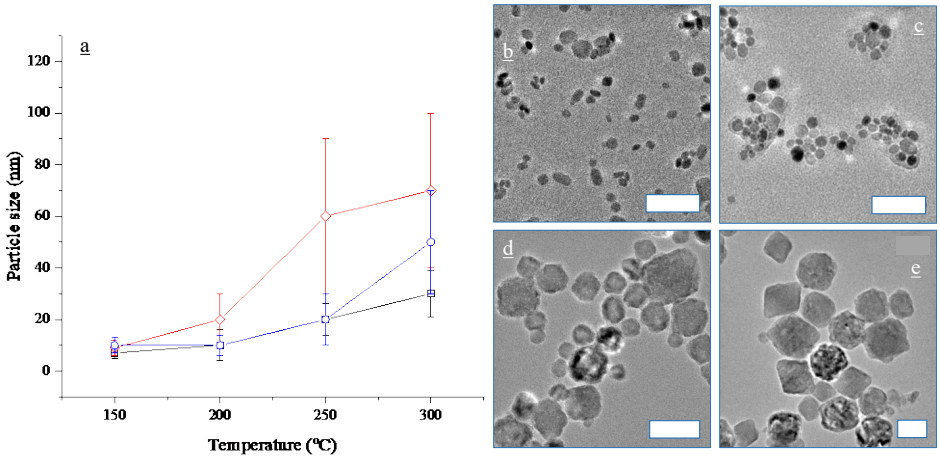

Figure 7. (a) Size distribution of nanoparticles produced after thermally decomposing $Mn(acac)_3$ in oleylamine. Squares, diamonds and circles correspond to reactions in N_2, N_2 with TMNO and air. Representative transmission electron microscopy images of products of the reactions under air, at (b) 150, (c) 200, (d 250, and (e) 300 °C. White scale bars correspond to 50 nm.

Conclusions:

This report clarifies the role of different synthetic conditions on the production of colloidal nanocrystals of MnO and Mn_3O_4 by thermolysis of $Mn(ac)_2$ or $Mn(acac)_3$ at elevated temperature in the presence of oleylamine, using a simple heat-up approach. It was found that only nanocrystals of MnO could be synthesized from $Mn(ac)_2$ precursor in a reaction solution that was carefully controlled to have no O_2 and H_2O contamination, with temperature only determining particle size and reaction kinetics. Conversely, when decomposing $Mn(acac)_3$ under inert conditions, nanocrystals of Mn_3O_4 were synthesized at or below 200 °C, whereas nanocrystals of MnO were the result of treatments above 250 °C if longer than 30 min. Regardless of precursor, oxidizing agents (air and TMNO) favored the formation of Mn_3O_4 nanocrystals at annealing temperatures of 150 and 200 °C. Therefore, temperature was the dominant factor affecting the composition of the product at annealing temperatures higher than 200 °C, regardless of the use of oxidizing agents and the oxidation state of the Mn precursor. Crystals of either of MnO and Mn_3O_4 smaller than 20 nm were generally reachable below 200 °C, whereas growth was rapid above this temperature. The data in this study provide a compendium that rationalizes seemingly contradicting observations in the literature. They highlight the importance of the control of the reaction environment to produce the desired phases. The study also provides strong indication that the formation of manganese oxides showing an average oxidation state of +3 or higher in colloidal form will require chemical creativity to move beyond unsaturated solvents and surfactants. The promise of a large new families of functional materials should provide motivation for the community to embark on this synthetic challenge.

Acknowledgements:

This work was supported as part of the Joint Center for Energy Storage Research (JCESR), an Energy Innovation Hub funded by the US Department of Energy, Office of Science, Basic Energy Sciences. Jannie M. Bolotnikov would like to thank the Honors College at the University of Illinois at Chicago for financial support.

Supporting Information Available:
This document includes powder X-ray diffraction patterns, images of reaction vessels,

transmission electron microscopy images and histograms of particle size distributions. This material is available free of charge via the Internet at http://pubs.acs.org.

References:

(1) Niederberger, M.; Pinna, N. *Metal Oxide Nanoparticles in Organic Solvents*; 2009.

(2) Burda, C.; Chen, X.; Narayanan, R.; El-Sayed, M. A. Chemistry and Properties of Nanocrystals of Different Shapes. *Chem. Rev.* **2005**, *105*, 1025–1102.

(3) Liu, X.; Chen, C.; Zhao, Y.; Jia, B. A Review on the Synthesis of Manganese Oxide Nanomaterials and Their Applications on Lithium-Ion Batteries. *J. Nanomater.* **2013**, 1–7.

(4) Xing, R.; Liu, G.; Quan, Q.; Bhirde, A.; Zhang, G.; Jin, A.; Bryant, L. H.; Zhang, A.; Liang, A.; Eden, H. S.; et al. Functional MnO Nanoclusters for Efficient SiRNA Delivery. *Chem. Commun.* **2011**, *47*, 12152–12154.

(5) Kwon, B. J.; Phillips, P. J.; Key, B.; Dogan, F.; Freeland, J. W.; Kim, C.; Klie, R. F.; Cabana, J. Nanocrystal Heterostructures of LiCoO2 with Conformal Passivating Shells. *Nanoscale* **2018**, *10*, 6954–6961.

(6) Sun, Y.; Liu, N.; Cui, Y. Promises and Challenges of Nanomaterials for Lithium-Based Rechargeable Batteries. *Nat. Energy* **2016**, *1*, 1–12.

(7) Liu, M.; Rong, Z.; Malik, R.; Canepa, P.; Jain, A.; Ceder, G.; Persson, K. A.; Liu, M. Spinel Compounds as Multivalent Battery Cathodes: A Systematic Evaluation Based on Ab Initio Calculations. *Energy Environ. Sci.* **2015**, *8*, 964–974.

(8) Kim, C.; Phillips, P. J.; Key, B.; Yi, T.; Nordlund, D.; Yu, Y. S.; Bayliss, R. D.; Han, S. D.; He, M.; Zhang, Z.; Burrell, A. K.; Klie, R. F.; Cabana, J. Direct Observation of Reversible Magnesium Ion Intercalation into a Spinel Oxide Host. *Adv. Mater.* **2015**, *27*, 3377–3384.

(9) Kim, C.; Adil, A. A.; Bayliss, R. D.; Kinnibrugh, T. L.; Lapidus, S. H.; Nolis, G. M.; Freeland, J. W.; Phillips, P. J.; Yi, T.; Yoo, H. D.; Kwon, B. J.; Yu, Y.-S.; Klie, R. F.; Chupas, P.; Chapman, K. W.; Cabana, J. Multivalent Electrochemistry of Spinel MgxMn3- XO4 Nanocrystals. *Chem. Mater.* **2018**, *30*, 1496–1504.

(10) Leite, E. R.; Ribeiro, C. *Crystallization and Growth of Colloidal Nanocrystals*; Springer: London, United Kingdom, 2012.

(11) Yin, M.; O'Brien, S. Synthesis of Monodisperse Nanocrystals of Manganese Oxides. *J. Am. Chem. Soc.* **2003**, *125*, 10180–10181.

(12) Jiao, F.; Harrison, A.; Bruce, P. G. Ordered Three-Dimensional Arrays of Monodispersed Mn3O4 Nanoparticles with a Core-Shell Structure and Spin-Glass Behavior. *Angew. Chemie - Int. Ed.* **2007**, *46*, 3946–3950.

(13) Seo, W. S.; Jo, H. H.; Lee, K.; Kim, B.; Oh, S. J.; Park, J. T. Size-Dependent Magnetic Properties of Colloidal Mn3O4 and MnO Nanoparticles. *Angew. Chemie - Int. Ed.* **2004**, *43*, 1115–1117.

(14) Zhang, H.; Jing, L.; Zeng, J.; Hou, Y.; Li, Z.; Gao, M. Revisiting the Coordination Chemistry for Preparing Manganese Oxide Nanocrystals in the Presence of Oleylamine and Oleic Acid. *Nanoscale* **2014**, *6*, 5918–5925.

(15) Sun, X.; Zhang, Y. W.; Si, R.; Yan, C. H. Metal (Mn, Co, and Cu) Oxide Nanocrystals

from Simple Formate Precursors. *Small* **2005**, *1*, 1081–1086.

(16) Ould-Ely, T.; Prieto-Centurion, D.; Kumar, A.; Guo, W.; Knowles, W. V.; Asokan, S.; Wong, M. S.; Rusakova, I.; Lüttge, A.; Whitmire, K. H. Manganese(II) Oxide Nanohexapods: Insight into Controlling the Form of Nanocrystals. *Chem. Mater.* **2006**, *18*, 1821–1829.

(17) Xie, S.; Zhou, X.; Han, X.; Kuang, Q.; Jin, M.; Jiang, Y.; Xie, Z.; Zheng, L. Supercrystals from Crystallization of Octahedral MnO Nanocrystals. *J. Phys. Chem. C* **2009**, *113*, 19107–19111.

(18) Hyeon, T.; Su Seong Lee; Park, J.; Chung, Y.; Hyon Bin Na. Synthesis of Highly Crystalline and Monodisperse Maghemite Nanocrystallites without a Size-Selection Process. *J. Am. Chem. Soc.* **2001**, *123*, 12798–12801.

(19) Mourdikoudis, S.; Liz-Marzán, L. M. Oleylamine in Nanoparticle Synthesis. *Chem. Mater.* **2013**, *25*, 1465–1476.

(20) Murphy, C. J.; Buriak, J. M. Best Practices for the Reporting of Colloidal Inorganic Nanomaterials. *Chem. Mater.* **2015**, *27*, 4911–4913.

(21) Siddiqi, M. A.; Siddiqui, R. A.; Atakan, B. Thermal Stability, Sublimation Pressures and Diffusion Coefficients of Some Metal Acetylacetonates. *Surf. Coatings Technol.* **2007**, *201*, 9055–9059.

(22) Seo, W. S.; Shim, J. H.; Oh, S. J.; Lee, E. K.; Hur, N. H.; Park, J. T. Phase- and Size-Controlled Synthesis of Hexagonal and Cubic CoO Nanocrystals. *J. Am. Chem. Soc.* **2005**, *127*, 6188–6189.

(23) Hou, Y.; Xu, Z.; Sun, S. Controlled Synthesis and Chemical Conversions of FeO Nanoparticles. *Angew. Chemie - Int. Ed.* **2007**, *46*, 6329–6332.

Table of Contents Figure.

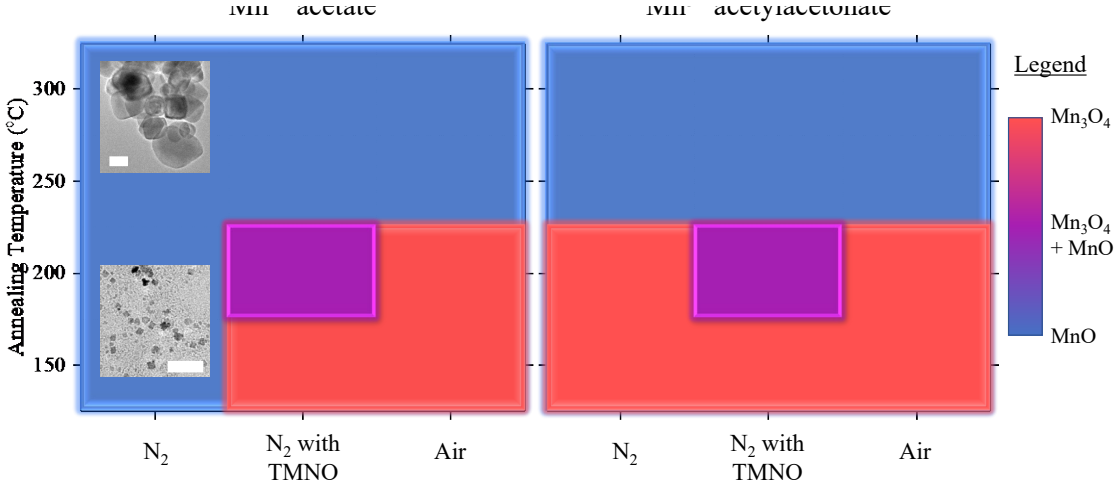

Table of Contents Synopsis. Nanocrystals of MnO and Mn_3O_4 have been synthesized by thermally decomposing Mn^{2+} acetate and Mn^{3+} acetylacetonate in oleylamine. It was found that MnO was favorable at annealing temperatures higher than 200 °C, regardless of the oxidation state of the precursor and oxidizing agent. By carefully removing O_2 and H_2O, MnO could be synthesized below 200 °C from Mn^{2+} acetate; otherwise, reactions generally favored the formation of Mn_3O_4. Scale bar measures 50 nm.